Improvement of fatigue crack growth resistance by controlled overaging in 2024-T3 aluminium alloy

A. TZAMTZIS and A. T. KERMANIDIS

Laboratory of Mechanics and Strength of Materials, Department of Mechanical Engineering, University of Thessaly, Volos, Greece

ABSTRACT   A controlled overaging process is proposed to increase region II fatigue crack propagation resistance of 2024-T3 aluminium alloy. Overaging was achieved by subjecting the material from the initial T3 state to heat treatment at specific aging temperatures resulting in substantial reduction in hardness. Fatigue crack growth tests were subsequently performed in the intermediate ΔK region to assess the influence of aging treatment on fatigue crack propagation rate. The experimental results showed that overaging at high temperatures enhances the fatigue crack growth resistance of the material with regard to initial T3 state. Fatigue crack growth rates were found to decrease with increasing overaging temperature. Cyclic stress strain tests were performed to assess the impact of the performed overaging on cyclic behaviour. The results revealed that cyclic strain hardening is enhanced in the overaged material, contributing to increased fatigue crack closure levels.

Keywords   aluminium alloy; crack closure; cyclic strain hardening; fatigue crack propagation; yield strength.

NOMENCLATURE
A_{25} = elongation at fracture
b = fatigue strength exponent
C = parameter of Paris equation
c = fatigue ductility exponent
E = Young's modulus
h = cyclic hardening capacity as a percentage increase of yield strength
H = strength coefficient
H' = cyclic strength coefficient
m = Paris equation exponent
n = strain hardening exponent
n' = cyclic strain hardening exponent
N_f = fatigue life
p = cumulated plastic strain
P_{max} = maximum applied load
P_{min} = minimum applied load
P_{op} = crack opening load
Q = maximum amount of hardening
R = stress/strain ratio
V = crack opening displacement at points A,B in C(T) specimen
V_{max} = crack opening displacement at points A,B in C(T) specimen corresponding at P_{max}
V_{min} = crack opening displacement at points A,B in C(T) specimen corresponding at P_{min}
V_{op} = crack opening displacement at points A,B in C(T) specimen when crack surfaces come into contact
β = driving rate of hardening
ΔV = crack opening displacement range at points A,B in C(T) specimen
$\Delta\varepsilon$ = total strain range
$\Delta\varepsilon_p$ = plastic strain range
ΔK = stress intensity factor range

Correspondence: A. Tzamtzis. E-mail: atzam@uth.gr

ΔK_{eff} = effective stress intensity factor range
$\Delta\sigma$ = stress range
ε_a^e = elastic strain amplitude
ε_a^p = plastic strain amplitude
ε'_f = fatigue ductility coefficient
ε_A = total strain amplitude
K_{op} = stress intensity factor corresponding to P_{op}
σ_0 = initial yield stress
$\sigma_{c0.2}$ = cyclic yield strength
σ'_f = fatigue strength coefficient
σ_{max} = maximum stress
σ_p = tensile peak stress
σ_{UTS} = tensile strength
σ_y = flow stress
$\sigma_{y0.2}$ = yield strength (offset 0.2%)

INTRODUCTION

Heat-treatable aluminium alloys offer, apart from high specific strength and ductility, good fatigue crack growth (FCG) resistance. Such characteristics are critical for lightweight applications with specific damage tolerance requirements under cyclic loads. Strength and ductility can be manipulated with the use of artificial aging.[1] The resulting microstructure may influence fatigue crack propagation performance, specifically in the near ΔK threshold region.[2–8] In the intermediate ΔK region (region II), microstructural influences become less important,[4,9,10] and FCG rates depend mainly on parameters, which influence cyclic deformation at the crack tip.[11–13]

The role of overaging close to peak-aged conditions on fatigue crack propagation has been a subject of research in several works. Overaging resulting in small hardness reduction relative to peak aging has been found to exhibit either negligible influence or a slight degradation in the fatigue crack propagation behaviour. In 2xxx series alloy, the FCG resistance of 2024 aluminium alloy in overaged state has been shown to exhibit small differences with regard to crack propagation rates near peak-aged conditions.[5,6] Garrett and Knott[14] examined the crystallographic nature of FCG in plate, pure Al-Cu alloys and showed that fatigue life after overaging was slightly shorter compared to peak-aged material. In 7xxx alloys, the FCG rate of overaged 7010 aluminium alloy was increased compared to the same material in peak-aged conditions.[15]

At higher aging temperatures, the degree of incoherency of particles increases, and coarsening of second-phase particles with non-shearable characteristics leads to reduction of strength.[16,17] Generally, for design purposes, this is not desirable. Simultaneously, the hardening behaviour, due to Orowan bypassing mechanism of semi- or incoherent particles, is modified.[16] Theoretical approaches on the effect of cyclic hardening on fatigue crack propagation have shown that with increasing cyclic hardening, crack closure levels under cyclic stresses increase as well.[18–20] However, existing experimental data to verify the behaviour are insufficient. In the present investigation, the influence of overaging associated with substantial reduction in strength on FCG behaviour of 2024 T3 alloy is experimentally examined, and the role of overaging on cyclic strain hardening characteristics is analysed.

EXPERIMENTAL PROCEDURE

Aging treatment and metallographic investigation
Material

Sheet, 2024 aluminium alloy with a thickness of 3.2 mm was used in T3 condition, which includes solution heat treatment at 495 °C, control stretching and natural aging. The nominal chemical composition of the alloy is in wt% Al-4.3Cu-1.5Mg-0.6Mn. The material was tested in the longitudinal (L) direction.

Heat treatment

For the selection of appropriate aging conditions, the overaging curves of the material were determined, which relate the reduction in hardness to the aging temperature and time. A heat treatment furnace with maximum heating capacity of 1200 °C was used, capable of maintaining a temperature accuracy of (±1 °C) during treatment. Small samples were placed inside the furnace and were artificially aged at temperatures ranging from 150 to 300 °C for periods up to 48 h. Subsequently, the overaging curves were used to obtain the microhardness variation with regard to aging parameters.

Microstructure

The material microstructure in initial T3 condition and after aging treatment was assessed using optical microscopy. Preparation of specimens for metallographic examination was made by grinding and polishing before etching. The specimens were etched with Keller's reagent, which consisted of 2 mL HF, 3 mL HCl, 5 mL HNO_3 and 190 mL H_2O.

Microhardness measurements

Microhardness measurements were performed in accordance with ASTM E92 standard.[21] The Vickers hardness values were determined on samples in T3 and overaged condition using an applied force of 200 g ($HV_{0.2}$).

Mechanical testing

Tensile tests

Tensile tests were conducted to obtain the mechanical properties of the material in T3 condition and after aging treatment. The tests were carried out on subsize specimens in the L material direction in accordance with ASTM E8M-01 specification.[22] In total, two specimens were tested in each aging condition, and average values of properties were obtained.

Fatigue crack growth tests

The fatigue crack propagation tests were carried out on compact tension C(T) specimens with a width of 60 mm in accordance with ASTM E647-00.[23] The notch was machined parallel to the rolling direction. The tests were performed on a 100 kN servo-hydraulic fatigue machine at room temperature, with a constant stress ratio of $R = 0.1$. The maximum stress was $\sigma_{max} = 10$ MPa and the frequency 5 Hz. A crack opening displacement gauge was used located at points A,B (Fig. 1), for crack opening measurements. Subsequently, data interpretation in terms of crack length was performed by implementation of the compliance method.
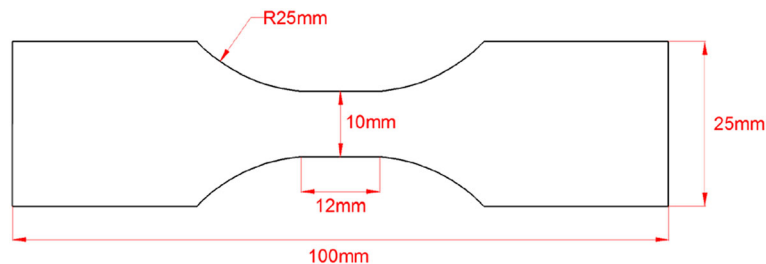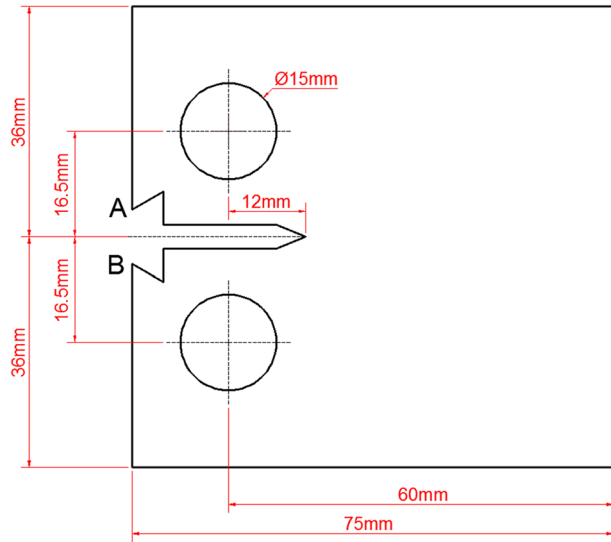

Fig. 1 C(T) specimen configuration according to specification ASTM E 647-00.

The crack growth characteristics were examined in T3 and overaged conditions. Crack growth rates were measured at an intermediate ΔK region ranging from 11 to 25 MPa$\sqrt{m}$. In total, 17 FCG tests were carried out, 6 for T3 and 11 for the two overaged conditions examined, to account for possible scatter effects.

Crack closure measurements were conducted in order to determine the minimum force at which the crack opens during cyclic loading in T3 and overaged conditions. The measurements were performed during fatigue testing using the compliance method according to ASTM E647-00.[23]

Strain-controlled fatigue tests

Strain-controlled fatigue tests were performed to assess the influence of overaging on cyclic hardening in accordance with the guideline SEP 1240.[24] The strain ratio was $R = -1$ and the frequency 0.2 Hz. The strain-controlled experiments were conducted using a dynamic axial clip-on extensometer (Fig. 2).

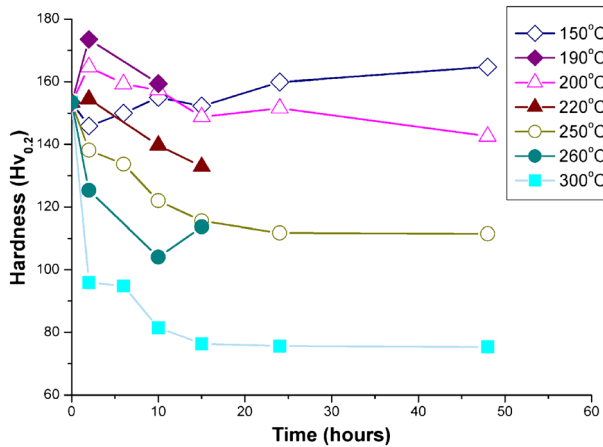**Fig. 2** Specimen configuration according to specification SEP 1240.

Fig. 3 Overaging curves of 2024-T3 aluminium alloy.

EXPERIMENTAL RESULTS

Overaging curves

The overaging curves are presented in Fig. 3 in terms of microhardness variation with aging parameters. The microhardness value in the initial T3 state was measured at 150 $HV_{0.2}$, which is in agreement with Ref. [1]. At temperatures below 200 °C, no significant decrease in microhardness was observed even at long aging times (~48 h). The maximum decrease of hardness was 50%

compared to the T3 state, at 300 °C for 10 h. At constant temperature, microhardness values were stabilized after approximately 15 h aging time. Based on the results of Fig. 3, specific aging parameters were selected, which lead to hardness reduction above 25% (which correspond to 250 and 300 °C). The aging time of 15 h was chosen as the threshold beyond which no significant hardness change was observed (Fig. 3). The materials produced with aging at 250 and 300 °C for 15 h, are referred to as A250 and A300 materials, respectively.

Microstructure

The microstructure in the T3 condition is shown in Fig. 4a. It consists of three types of inclusions: (i) Al-Cu containing particles; (ii) Al-Cu-Fe-Mn containing particles; and (iii) Al-Cu-Fe-Si-Mn containing particles as obtained from the performed scanning electron microscopy/energy dispersive X-ray spectroscopy analysis. The results are in agreement with the literature.[1,25,26] The 2024-T3 microstructure is characterized by two major second-phase particles: Al_2Cu (θ' phase) and Al_2CuMg (S phase).[25]

In Fig. 4b and c, the microstructures of the alloys A250 and A300 are displayed. Metastable phases have dissolved from the grain boundaries and precipitated within the grains. Precipitate-free zones are evident at the grain boundaries, and inside the grains, coarsening
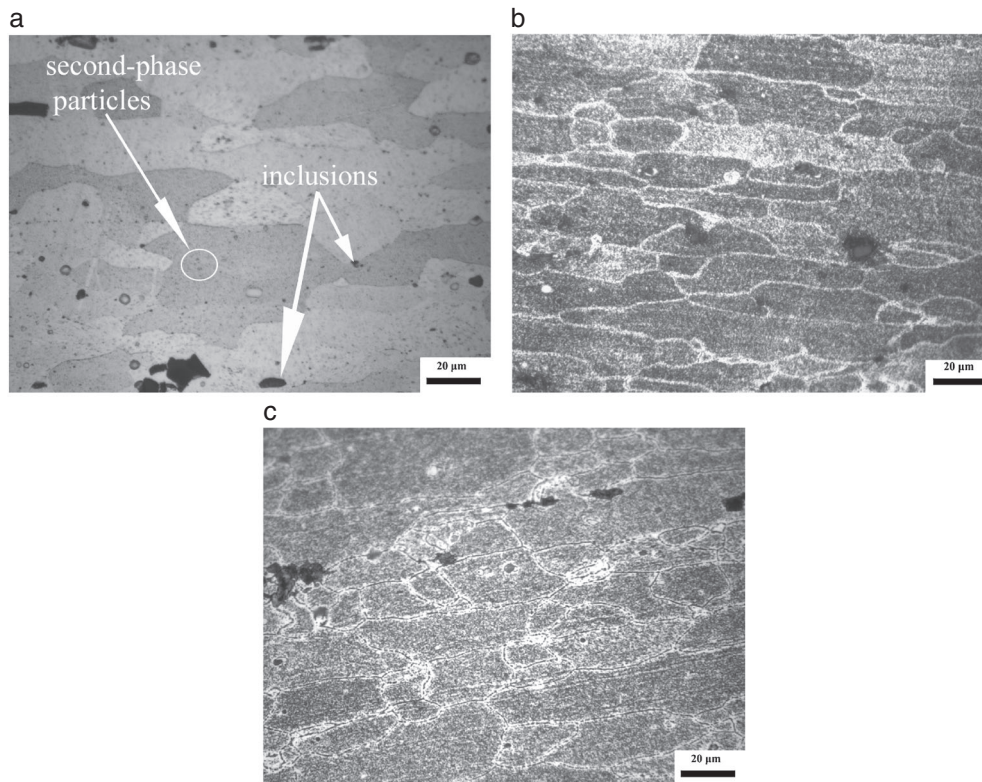

Fig. 4 Microstructures of (a) reference T3 material and materials subjected to artificial aging (b) A250 and (c) A300.

of the metastable phases can be observed. Inclusions seem to be unaffected. Coarsening of metastable phases in the alloy A300 is more pronounced compared to the alloy A250. The aforementioned observation is consistent with the decreased hardness values of A300 alloy compared to A250.

Tensile tests

The tensile properties of the materials are given in Table 1 and the engineering tensile stress–strain curves, for the different aging conditions, are shown in Fig. 5. A gradual decrease in yield strength with aging temperature is observed. The percentage reduction is 36% in A250 and 64% in A300 material with respect to the initial value (T3). The elongation at failure is approximately the same for the two overaging conditions examined and corresponds to 30% reduction with regard to the T3 state.

Fatigue crack growth

In Figs 6 and 7, the FCG results of the materials are compared showing a pronounced effect of aging treatment on FCG behaviour. Specifically, FCG resistance is enhanced after overaging treatment and increases with the magnitude of overaging temperature. For better clarity, only two characteristic tests are presented from the total number of specimens for each material, in Figs 6a and 7. The characteristic crack growth curves were chosen

Table 1 Tensile test results

	Yield strength $\sigma_{y\,0.2}$ (MPa)	Elongation at fracture A_{25} (%)	Tensile strength σ_{UTS} (MPa)
T3	375	15	490
A250	240	10	355
A300	135	11	285
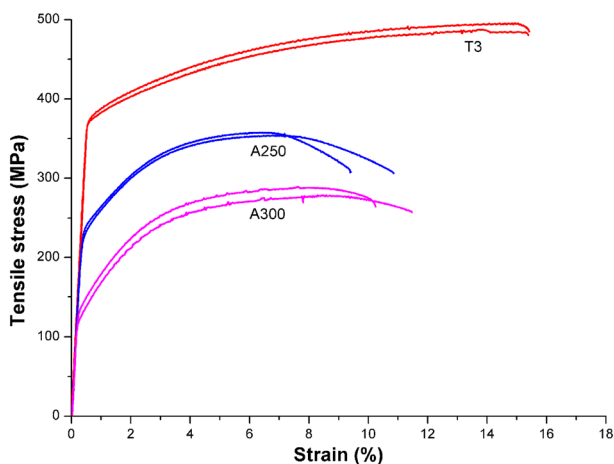
Fig. 5 Tensile stress–strain curves of T3, A250 and A300 materials.

for each case based on two samples exhibiting experimental fatigue lives closer to the mean fatigue life value of the series. Fatigue lives were assessed considering the experimental scatter in fatigue life measurements. In Fig. 6b, the experimental fatigue lives, corresponding to fracture of specimen, are plotted as mean values with the standard deviation for each material. Including the effect of scatter in the results, the observed trends in FCG behaviour, showing degradation of FCG resistance with aging temperature, are not affected. FCG rates of T3 and overaged materials are compared in Fig. 7. Crack growth rates in A250 and A300 materials are lower than in T3 material in the whole ΔK range examined, with A300 exhibiting superior crack growth resistance. The effect is more noticeable in the lower ΔK range between 12 and 15 MPa$\sqrt{m}$.

The Paris equation constants were determined from the experimental results and are presented in Table 2. The value of parameter C decreases with increasing aging temperature, which is consistent with the lower crack growth rates in the overaged material described previously.

Crack closure measurements

Measurements of crack closure during fatigue testing are presented in Fig. 8a in terms of normalized crack opening load (P_{op}/P_{max}) versus the applied stress intensity factor range ΔK. The maximum force P_{max} was constant during the test with a value of 10.92 kN. The magnitude of crack closure increases steeply with increasing overaging temperature in the range 11–15 MPa$\sqrt{m}$, reaching a level of crack closure that is dependent on the overaged state and corresponds to highest closure levels for A300 material. The higher levels of closure after overaging are in agreement with the lower C values shown in Table 2 (taking into account that variation of parameter m between the materials is small) and justify the lower FCG rates of Fig. 7.

In Fig. 8b, crack opening values V (measured at points A,B in C(T) specimen), normalized with respect to the maximum crack opening value V_{max}, are plotted against the applied force. Specifically, values of V versus load are displayed during one unloading event within the cyclic loading history, at crack lengths 15.5 mm ($\Delta K = 11.5$ MPa$\sqrt{m}$) and 19 mm ($\Delta K = 14$ MPa$\sqrt{m}$) for T3 and A300 materials. During unloading, the crack is fully open, and a linear relation between force and displacement exists, which is dependent only on the elastic properties (Young's modulus), and hence, the curves for both materials coincide. At lower values of applied force P, the crack surfaces come into contact, and the force–displacement diagram becomes nonlinear. At onset of nonlinearity, the values of V and P become V_{op} and P_{op}. As shown in Fig. 8b, V_{op} for A300 is increasing with increasing crack length, while for T3 material, the respective increase is very small. In particular, V_{op} was
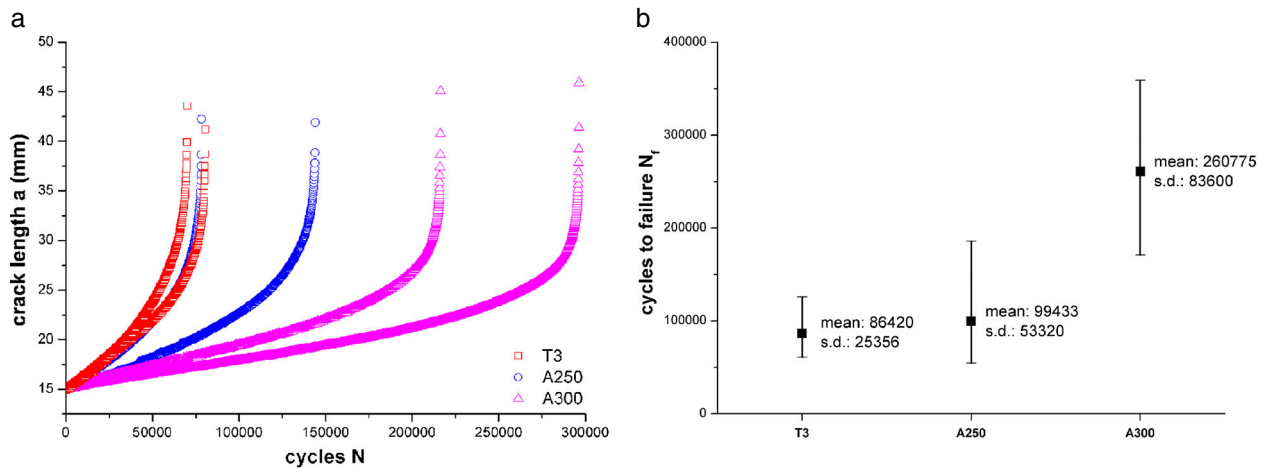
Fig. 6 (a) Constant stress amplitude crack growth curves of T3, A250 and A300 materials for maximum stress $\sigma_{max} = 10$ MPa and stress ratio $R = 0.1$ (b) Fatigue lives obtained from (a–N) curves given as mean values with standard deviation (s.d.).
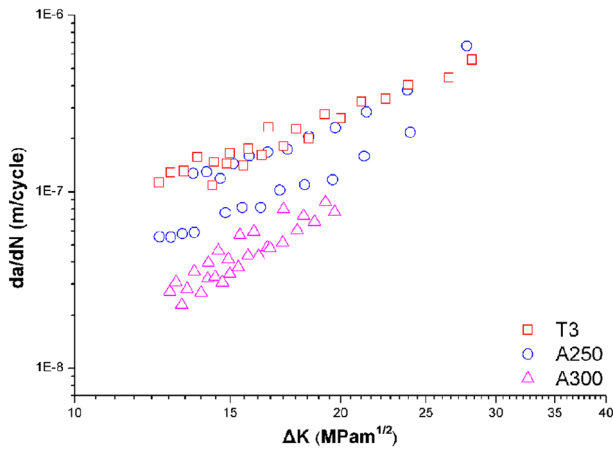

Fig. 7 Fatigue crack growth rates versus stress intensity factor range ($\mathrm{d}a/\mathrm{d}N$–ΔK) in T3, A250 and A300 materials.

determined 0.076 and 0.14 mm for A300 and 0.060 and 0.075 mm for T3 material at crack lengths 15.5 and 19 mm, respectively. Also, during unloading, the decrease in slope after V_{op} is more pronounced for the A300 material, which results in higher V_{min} values (for applied P_{min}) with increasing crack length. The V_{min} values are 0.033 and 0.049 mm for A300, and 0.025 and 0.032 mm for T3 material at crack lengths 15.5 and 19 mm, respectively. Hence, the decrease of crack opening range $\Delta V = V_{max} - V_{min}$ for A300 with advancing crack size is higher compared to T3. The decrease in ΔV is in line with the increase in closure in the range 11–15 MPa$\sqrt{\mathrm{m}}$ (Fig. 8a) for A300. The previous analysis is used in the Section on Cyclic Hardening Behaviour for the assessment of the role of hardening behaviour on the crack closure in the range 11–15 MPa$\sqrt{\mathrm{m}}$.

Table 2 Paris constants calculated for the materials under investigation

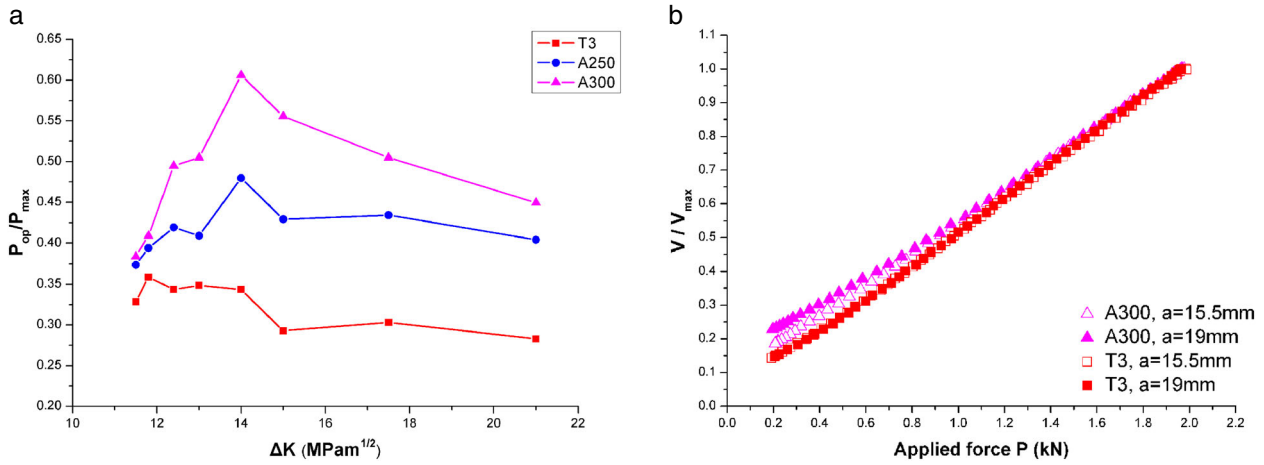|	Specimen number	Parameter m		Parameter C	
T3	1	10.78	Mean value: 2.01	1.9×10^{-9}	Mean value: 7.51×10^{-10}
	2	2.15		2.24×10^{-10}	
	3	2.19		3.5×10^{-10}	
	4	1.8		8.55×10^{-10}	
	5	1.93		8.88×10^{-10}	
	6	2.21		2.93×10^{-10}	
A250	1	1.89	Mean value: 2.17	1.44×10^{-9}	Mean value: 5.93×10^{-10}
	2	2.64		5.59×10^{-11}	
	3	2.01		9.83×10^{-10}	
	4	2.26		3.63×10^{-10}	
	5	2.34		2.29×10^{-10}	
	6	1.88		4.88×10^{-10}	
A300	1	2.91	Mean value: 2.72	1.18×10^{-11}	Mean value: 2.96×10^{-11}
	2	2.51		5.24×10^{-11}	
	3	2.85		1.57×10^{-11}	
	4	2.51		5.24×10^{-11}	
	5	2.85		1.57×10^{-11}	

Fig. 8 (a) Variation of crack closure as a function of applied stress intensity range, in T3 and overaged materials; (b) crack opening values versus applied force during an unloading event within the cyclic loading history for T3 and A300 materials. The crack opening values correspond to crack lengths 15.5 and 19 mm.

In Fig. 9, the FCG rates are compared for all materials using the effective stress intensity factor range ΔK_{eff} according to Eq. 1. ΔK_{eff} was calculated according to Ref. [23], where K_{op} is the stress intensity factor for the measured P_{op}. For the calculation of K_{op}, a mean level of P_{op} in the range 11–21 MPa$\sqrt{m}$ was used. The mean level values of P_{op} were 0.65, 0.85 and 1 kN for T3, A250 and A300 materials, respectively. With consideration of ΔK_{eff} values, crack growth rate levels are converging in a narrow band, which demonstrates the influence of crack closure on FCG rates.

$$\Delta K_{eff} = K_{max} - K_{op}. \qquad (1)$$

The results of Fig. 8 are in agreement with the fact that crack closure is generally more dominant at lower ΔK levels.[2] Crack closure levels determined experimentally increase with the magnitude of aging temperature, which rationalizes the FCG performance observed in Figs 6 and 7.
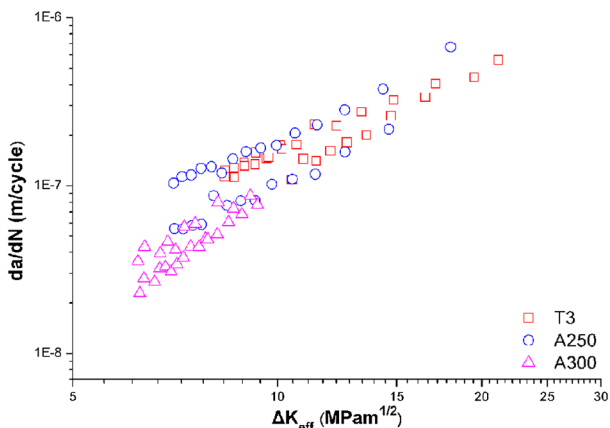

Fig. 9 Fatigue crack growth rates versus effective stress intensity factor range ($da/dN–\Delta K_{eff}$) in T3 and overaged materials.

Fractography

Fractographic analysis was performed to evaluate specific fracture characteristics during fatigue crack propagation. In the micrographs of Fig 10a and b taken with optical stereoscope, segments of fracture surfaces for T3 and A300 materials are presented. The fracture characteristics of A300 material are more brittle compared to T3 and are characterized by radiating ridges from the notch tip, sign of the crack changing slip planes during crack growth.[27] Thus, the fracture path in A300 includes more surface irregularities than T3, which are expected however to have small contribution to the measured crack closure levels in the intermediate ΔK region. This effect has been shown to be significant in microstructures with variations in grain morphology characteristics,[28,29] which is not the case in the present study.

In the micrographs of Figs 11a and b, fracture surfaces of T3 and A300 materials taken with scanning electron microscope are displayed. The micrographs show a semi-cleavage fracture pattern in T3 alloy consisting of dimples as well as cleavage facets (Fig. 11a). Fracture surfaces of A300 material included larger brittle regions compared to T3 (Fig. 11b). The fracture characteristics in the overaged alloy agree with the lower fracture toughness values obtained in A300 compared to T3 alloy in a previous work by the present authors.[30] The more brittle behaviour in the overaged alloy combined with the lower crack growth rates suggests that cyclic strain hardening should be the more contributing factor on crack closure rather than the accumulation of plastic strains at the crack tip. Cyclic strain hardening reduces the ability of the material to plastically deform at the crack front. According to the work of Pommier,[19] this has been associated with
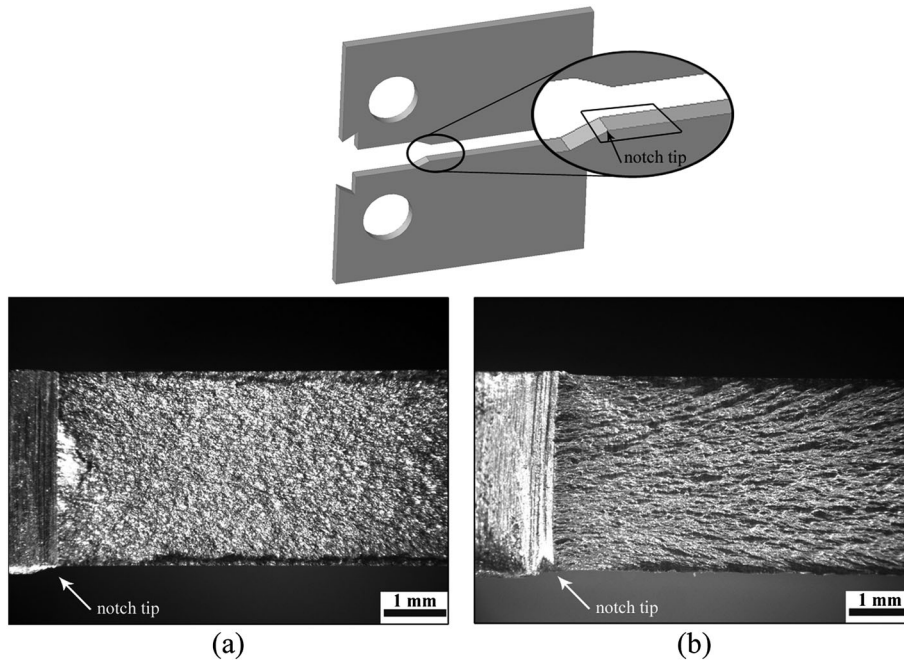
Fig. 10 Fracture surface characteristics during FCG in (a) T3 and (b) A300 materials.
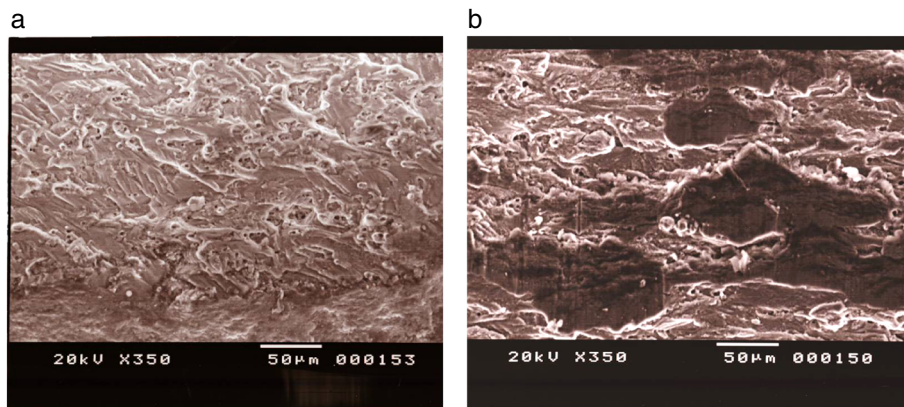

Fig. 11 Scanning electron microscopy images showing fracture surface characteristics during FCG in (a) T3 and (b) A300 conditions.

extension of the plastic deformation to the back of the crack tip enhancing crack closure. The role of overaging on cyclic strain hardening is studied in the next paragraph and compared to the hardening behaviour in T3 state.

Influence of overaging on cyclic strain hardening
Cyclic stress–strain behaviour

In Fig. 12a, the experimental strain–life curves for A300 and T3 materials are shown. In the figure, fatigue lives are displayed with regard to the total strain amplitude ε_A. For determining fatigue life N_f, the failure criterion was considered the fracture of the specimen. The total strain amplitude is given as the sum of elastic and plastic parts using the Basquin and Coffin–Manson equations, respectively, in the form

$$\varepsilon_{\mathrm{A}} = \frac{\Delta\varepsilon}{2} = \frac{\sigma_f'}{E}\left(2N_f\right)^b + \varepsilon_f'\left(2N_f\right)^c. \tag{2}$$

The experimental constants of the equations in both elastic and plastic regions are given in Fig. 12. In the low cycle fatigue (LCF) region (Fig. 12c), where plastic strains are dominant, fatigue lives are higher in A300 material compared to T3. On the contrary, fatigue lives in the high cycle fatigue (HCF) region (Fig. 12b) are superior in the T3 aluminium alloy.

a

$\varepsilon_A = 375/72000*(2N_f)^{-0.082} + 0.25(2N_f)^{-0.65}$, (A300)

$\varepsilon_A = 1203/72000*(2N_f)^{-0.146} + 0.13(2N_f)^{-0.79}$, (T3)

■ T3
○ A300

b

$\varepsilon_a^e = 1203/72000*(2N_f)^{-0.146}$, (T3)

$\varepsilon_a^e = 375/72000*(2N_f)^{-0.082}$, (A300)

■ T3
○ A300

c

$\varepsilon_a^p = 0.25(2N_f)^{-0.65}$, (A300)

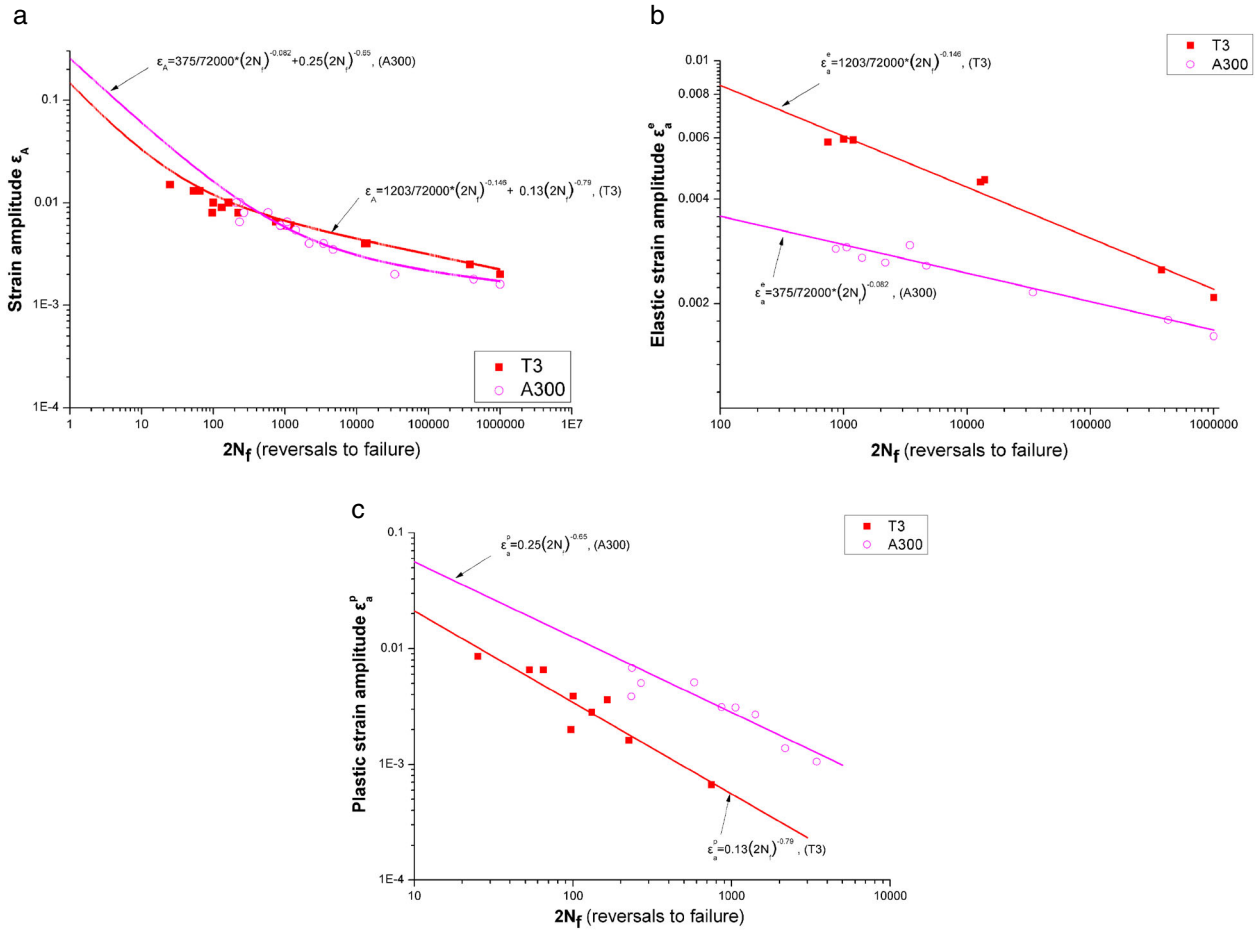$\varepsilon_a^p = 0.13(2N_f)^{-0.79}$, (T3)

■ T3
○ A300

Fig. 12 Strain–life curves of T3 and A300 materials for strain ratio $R = -1$ plotted in terms of (a) total, (b) elastic and (c) plastic strain amplitude.

In Fig. 13, the cyclic stress strain curves for A300 and T3 alloy up to a strain range level of 1.25% are shown. Both materials exhibit cyclic strain hardening with the cyclic curve positioned above the respective monotonic
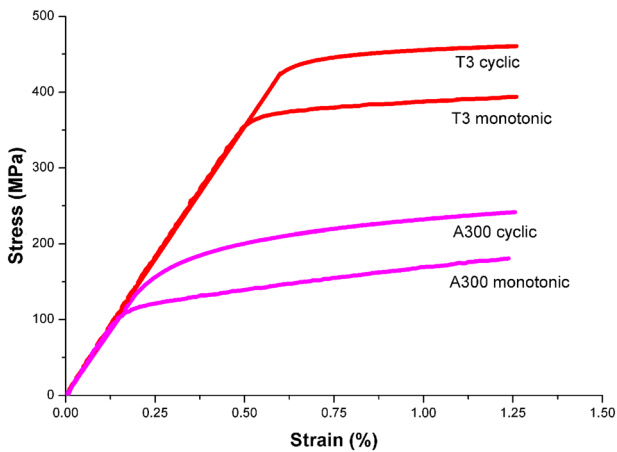
T3 cyclic
T3 monotonic
A300 cyclic
A300 monotonic

Fig. 13 Monotonic and cyclic stress–strain curves of T3 and A300 materials for strain ratio $R = -1$.

behaviour. Calculation of the 0.2% cyclic yield strength value ($\sigma_{c0.2}$) revealed an increase in yield strength due to cyclic hardening of 37% and 16% of A300 and T3 materials, respectively, compared to the monotonic behaviour. For a plastic strain level of 0.6%, the respective increase of stress due to cyclic hardening was 42% for A300 material and 17% for T3 material. The cyclic strain hardening exponent n' and cyclic strength coefficient H' were assessed with the Ramberg–Osgood equation (Eq. 3)[31]:

$$\frac{\Delta \varepsilon}{2} = \frac{\Delta \sigma}{2E} + \left(\frac{\Delta \sigma}{2H'}\right)^{1/n'}. \tag{3}$$

The constants are given in Table 3 together with the respective n and H values for the monotonic behaviour.

In Fig. 12a, a small deviation is observed between the strain–life curve (ε–N) of T3 material (sum of the elastic and plastic strain curves) and the experimental data in the LCF region. This deviation occurs because at very high plastic strain amplitudes, resulting in significantly

Table 3 Strain hardening exponent and strength coefficient for monotonic and cyclic behaviour

	n	H (MPa)	n'	H' (MPa)
T3	0.08	580	0.0211	512.8
A300	0.23	530	0.131	446.7

large total strains, the evolution of maximum stress reaches a saturated value (see cyclic stress strain curve, Fig. 13). In this region, the elastic strain component does not change significantly with increasing total strain amplitude. Therefore, in the mentioned LCF region, the Basquin equation of T3 material overestimates the applied elastic strains, leading to a small shift of the ε–N curve to higher strain levels. In the case of A300, at high strain amplitudes, a smaller level of maximum stress saturation exists (Fig. 13), and the deviation obtained with Basquin prediction for the elastic component is less pronounced.

In Fig. 14a and b, the cyclic test results for T3 and A300 materials are compared for plastic strain range levels 0.2% and 0.45%. Tension and compression stress peaks increase with the number of cycles, with the compression curve lying on or slightly above the respective tension curve, indicating the absence of Bauschinger effect. During the initial phase of cyclic deformation, cyclic hardening occurs, leading to an increase in tensile peak stresses σ_p, followed by an extended phase of maximum cyclic stress saturation N_{sat} (during which stresses present a variation of less than 2.5%). The fatigue lives obtained for both strain levels are higher for A300 material, an indication of higher cyclic plastic strain resistance compared to the T3 material. The hardening magnitude (percentage increase in stress amplitude) has been determined for the $N_{hardening}$ phase, which precedes the N_{sat} phase, as shown in Fig. 14. For 0.2% plastic strain range, the stress amplitude increase is 11% in the T3 material, at the stabilized cyclic stress–strain behaviour, whereas in the overaged material, the increase is 25%. At 0.45% plastic strain range, the

respective $\Delta\sigma$ increase is 17% for the T3 material and 26% for the overaged material. At 0.2% plastic strain range, the damage stage correlated with fatigue crack initiation (N_{ini}) is noticeable at the end of the N_{sat} phase, where a drop in maximum stresses is observed. At 0.45% plastic strain range, the respective crack initiation period was very small, and sudden fracture occurred at the end of the N_{sat} phase.

Taking into account that the crack initiation phase N_{ini} is small compared to the total fatigue life under cyclic plastic straining, the higher N_f values under LCF conditions obtained in Figs 12c and 14 for the overaged alloy indicate a retardation of crack initiation compared to T3 material, under the same plastic strain levels. In the HCF regime, the effect of the proposed overaging treatment on the resistance to crack initiation is unknown, but likely inferior with respect to the T3 condition, where fatigue lives obtained for the T3 alloy are higher compared to A300, as shown in Fig. 12b. The observed material behaviour combined with the results of Fig. 7 presents useful information for damage tolerance design in applications involving stress concentration regions (e.g. rivet holes and geometrical discontinuities). When a crack initiates around stress concentration regions, crack initiation is followed by a sudden transition to medium ΔK conditions of the advancing crack, considering its increase in size due to the imperfection width (e.g. hole diameter). In the vicinity of such structural details, plastic strains prevail, and therefore, LCF material conditions may be considered applicable. Because LCF behaviour in the overaged state has been found to be superior with regard to T3 condition, it should be expected that crack initiation is favoured under such conditions after overaging.

Cyclic hardening behaviour

Taking into account the hardening behaviour presented in Fig. 12 and in order to estimate in more detail the cyclic hardening response (evolution of initial flow stress σ_y
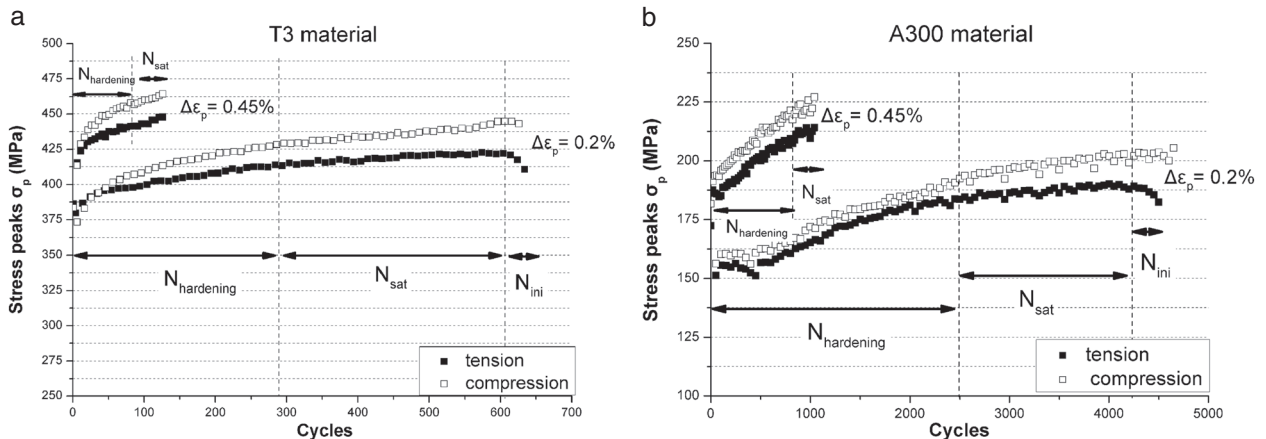
Fig. 14 Cyclic test results under constant plastic strain range of 0.2% and 0.45% for (a) T3 and (b) A300 materials.
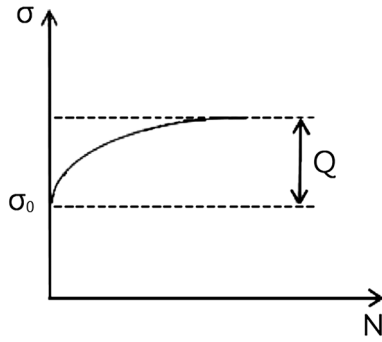
Fig. 15 Evolution of yield stress taking into account the hardening capacity Q.

with the number of cycles), a nonlinear, isotropic hardening behaviour has been implemented according to Ref. [19] in the form

$$\sigma_y = \sigma_0 + Q\left(1 - e^{-\beta p}\right), \qquad (4)$$

where σ_0 is the initial yield stress value corresponding to the applied plastic strain level of the material, parameters Q and β are the maximum amount of hardening and driving rate of hardening, respectively, and p is the cumulated plastic strain. In Fig. 15, a schematic representation of the evolution of yield stress with the number of cycles N taking into account the isotropic parameter Q is given.

The cumulated plastic strain p, in a uniaxial, fully reversed strain-controlled test, can be approximated (by assuming that the plastic strain range is constant) as $p = N\Delta\varepsilon_p$, where $\Delta\varepsilon_p$ is the plastic strain range in each cycle and N the number of cycles applied. Substituting p into Eq. 4 results in the following expression:

$$\sigma_y = \sigma_0 + Q\left(1 - e^{-\beta N\Delta\varepsilon_p}\right). \qquad (5)$$

The amount of hardening can be defined as follows[19]:

$$h = \frac{\sigma_0 + Q}{\sigma_0}. \qquad (6)$$

Parameter h describes the cyclic hardening capacity of the material, as a percentage increase of cyclic yield strength. With implementation of Eq. 5 as a fitting function on the cyclic hardening curves (Fig. 14), isotropic parameters σ_0, Q, h and β have been determined, for the case of tensile stress peaks, and are presented in Table 4. A typical fitting curve describing the evolution of σ_y with the number of cycles using Eq. 5 for the case of 0.2% plastic strain range is shown in Fig. 16.

In Ref. [19], an increase of parameter h has been associated with an increase of crack closure levels under cyclic loading. In the present investigation, parameter h has been found higher for A300 compared to T3 material. From Table 4, h was found to be 1.11 for T3 and 1.25 for A300 material at a plastic strain range 0.2%, while for 0.45%, it was found 1.17 and 1.26, respectively. The aforementioned results combined with the fact that cyclic

Table 4 Isotropic hardening parameter values for A300 and T3 materials

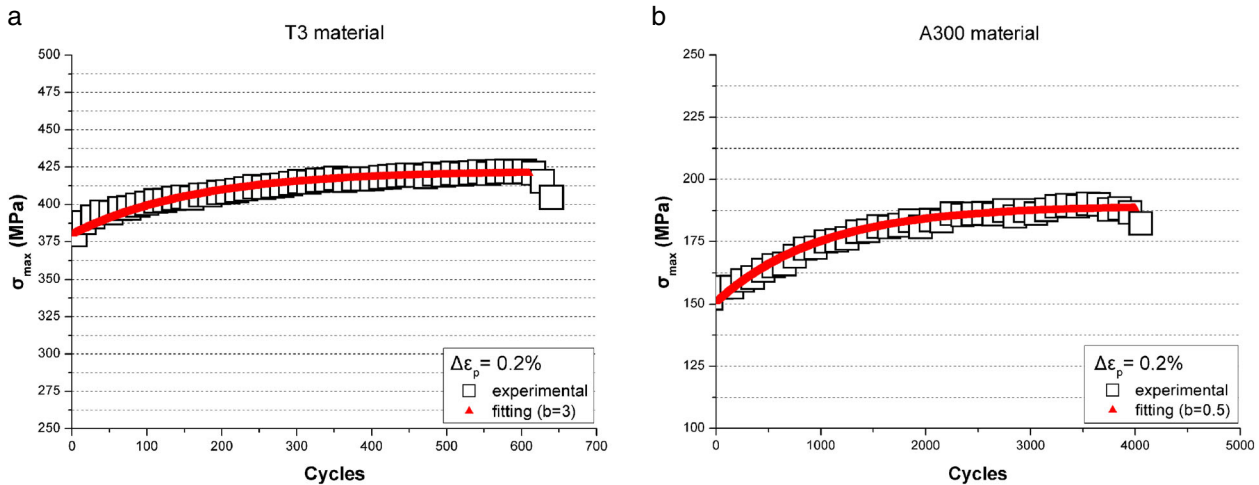| $\Delta\varepsilon_p$ (%)	Material	σ_0 (MPa)	Q (MPa)	h	β
0.2	T3	380	42	1.11	3
	A300	151	38	1.25	0.5
0.45	T3	386	68	1.17	7
	A300	172	45	1.26	0.4

a

b

Fig. 16 Cyclic test results under constant plastic strain range 0.2% and fitting curves of (a) T3 and (b) A300.

strain hardening exponent n' increases in A300 material confirm the higher cyclic hardening capacity and may explain the higher crack closure level of the overaged material with respect to T3 alloy. Furthermore, the aforementioned results provide further insight on the dissimilar increase in crack closure in the range 11–15 MPa$\sqrt{m}$ described in Fig. 8. As discussed in the Section on Crack Closure Measurements, the crack opening range $\Delta V = V_{max} - V_{min}$ is decreasing in a larger extent in the overaged alloy with increasing crack length with respect to T3. This should be expected, since a material volume at the crack tip subjected to a fixed load amplitude, exhibits a decrease of strain range with loading cycles, when cyclic hardening is present and the magnitude of decrease is related to the amount of cyclic hardening. For higher ΔK values, the crack increases in size, V_{max} increases significantly and the contribution of the above effects on ΔV and closure is less pronounced. In the present study, possible combined influences of hardening effects and residual stresses due to small-scale plasticity at the crack tip have not been taken into account, and further investigation is essential to determine how these mechanisms interact and affect closure in the overaged state.

CONCLUSIONS

The 2024 T3 aluminium alloy was heat treated at specific overaging temperatures to produce alloy with substantial decrease in hardness. The effect of selected overaging conditions on fatigue crack propagation behaviour as well as on the cyclic behaviour was investigated experimentally. The experimental findings showed the following:

- FCG rates were lower in the overaged material and were associated with higher crack closure levels compared to T3 alloy. Reduction in FCG rates was higher with increasing overaging temperature.
- Cyclic strain tests showed that the overaged material exhibits superior fatigue behaviour in the LCF region, while the T3 alloy showed increased fatigue resistance in the HCF region.
- The role of modified, due to overaging, cyclic strain hardening behavior on the dissimilar levels of crack closure has been investigated. A nonlinear isotropic hardening behaviour was implemented to describe cyclic strain hardening characteristics. The amount of cyclic hardening for the overaged material was higher compared to the 2024 T3 alloy.

Acknowledgements

REFERENCES

1 Kaufman, J. G. (2000). Introduction to Aluminum Alloys and Tempers. ASM International, Ohio.

2 Suresh, S. (1998). Fatigue of Materials. 2nd edn, Cambridge University Press, London, UK.

3 Lindigkeit, J., Terlinde, G., Gysler, A. and Lutjering, G. (1979). The effect of grain size on fatigue crack propagation behavior of age-hardened alloys in inert and corrosive environment. *Acta Metall.*, **27**, 1717-1726.

4 Davidson, D. L. and Lankford, J. (1992). Fatigue crack growth in metals and alloys: mechanisms and micromechanics. *Int. Mater. Rev.*, **37**, No2, 45-76.

5 Bray, G. H., Glazov, M., Rioja, R. J., Li, D. and Gangloff, R. P. (2001). Effect of artificial aging on the fatigue crack propagation resistance of 2000 series aluminum alloys. *Int. J. Fatig.*, **23**, 265-276.

6 Sarioglu, F. and Orhaner, F. O. (1998). Effect of prolonged heating at 130°C on fatigue crack propagation of 2024 Al alloy in three orientations. *Mater. Scie. Eng. A*, **248**, 115-119.

7 Sharma, V. M. J., Kumar, K. S., Rao, B. N. and Pathak, S. D. (2011). Fatigue crack growth of AA2219 under different aging conditions. *Mater. Sci. Eng. A*, **528**, 4040-4049.

8 Zaiken, E. and Ritchie, R. O. (1985). Effects of microstructure on fatigue crack propagation and crack closure behavior in aluminum alloy 7150. *Mater. Sci. Eng.*, **70**, 151-160.

9 Grinberg, N. M. (1984). Stage II fatigue crack growth. *Int. J. Fatigue*, **6**, No 4, 229-242.

10 Roven, H. J. and Nes, E. (1991). Cyclic deformation of ferritic steel – II. Stage II crack propagation. *Acta metal. Mater.*, **39**, No 8, 1735-1754.

11 Kumar, R. and Garg, S. B. L. (1989). Effect of yield stress and stress ratio on fatigue crack closure in 6063-T6 aluminium alloy. *Int. J. Pres. Ves. & Piping*, **38**, 293-307.

12 Putatunda, S. K. (1988). Influence of material strength level on fatigue crack closure. *Eng. Fract. Mech.*, **30**, No 5, 627-639.

13 Petrak, G. J. (1974). Strength level effects on fatigue crack growth and retardation. *Eng. Fract. Mech.*, **6**, 725-733.

14 Garret, G. G. and Knott, J. F. (1975). Crystallographic fatigue crack growth in aluminium alloys. *Acta Metall.*, **23**, 841-848.

15 Desmukh, M. N., Pandey, R. K. and Mukhopadhyay, A. K. (2006). Effect of aging treatments on the kinetics of fatigue crack growth in 7010 aluminum alloy. *Mater. Sci. Eng. A*, **435-436**, 318-326.

16 Simar, A., Brechet, Y., Meester, B. de, Denquin, A. and Pardoen, T. (2007). Sequential modeling of local precipitation, strength and strain hardening in friction stir welds of an aluminum alloy 6005A-T6. *Acta Mater.*, **55**, Issue 18, 6133-6143.

17 ASM Handbook Volume 4 (1991). Heat Treating, ASM International, Ohio.

18 Budiansky, B. and Hutchinson, J. W. (1978). Analysis of closure in fatigue crack growth. *J. Appl. Mech.*, **45**, No. 2, 267-275.

19 Pommier, S. (2002). Plane strain crack closure and cyclic hardening. *Eng. Fract. Mech.*, **69**, 25-44.

20 Chang, T. and Guo, W. (1999). Effects of strain hardening and stress state on fatigue crack closure. *Int. J. Fatig.*, **21**, 881-888.

21 ASTM E92 (2003). Standard test methods for Vickers hardness of metallic materials. Annual Book of ASTM Standards, American Society for testing and Materials, Philadelphia (PA).

22 ASTM E8M (2001). Standard test methods for tension testing of metallic materials. Annual Book of ASTM Standards, American Society for testing and Materials, Philadelphia (PA).

23 ASTM E647 (2000). Standard test method for measurement of fatigue crack growth rates. Annual Book of ASTM Standards, American Society for testing and Materials, Philadelphia (PA).

24 SEP 1240 (2006). Testing and Documentation Guideline for the Experimental Determination of Mechanical Properties of Steel Sheets for CAE Calculations, 1st edn, Institute VDEh, Dusseldorf, Germany.

25 Huda, Z., Taid, N. I. and Zaharinie, T. (2009). Characterization of 2024-T3: an aerospace aluminum alloy. *Mater. Chem. Phys.*, **113**, 515–517.

26 ASM Handbook Volume 2 (1990). Properties and Selection: Nonferrous Alloys and Special-Purpose Materials. ASM International, Ohio.

27 Callister, W. D., Rethwisch, D. G. (2010). Materials Science and Engineering: An Introduction. 8th edn, Wiley, USA.

28 Kermanidis, A. T. and Pantelakis, Sp. G. (2011). Prediction of crack growth following a single overload in aluminum alloy with sheet and plate microstructure. *Eng. Fract. Mech.*, **78**, Issue 11, 2325-2337.

29 Venkateswara, K. T., Bucci, R. J., Jata, K. V. and Ritchie, R. O. (1991). A comparison of fatigue crack propagation behavior in sheet and plate aluminum-lithium alloys. *Mater. Sci. Eng. A*, **141**, 39-48.

30 Kermanidis, A. T. and Tzamtzis, A. (2012). Prediction of fatigue crack propagation in aluminum alloy with local yield strength gradient at the crack path. *Proceedings of 14th International Conference on Mesomechanics*, Budapest, Hungary.

31 Dowling, N. E. (2006). Mechanical Behavior of Materials: Engineering Methods fir Deformation, Fracture, and Fatigue. 3rd edn, Prentice Hall, USA.